Macromolecules

Article

pubs.acs.org/Macromolecules

Mechanical Properties and Degradation of Chain and Step-Polymerized Photodegradable Hydrogels

Mark W. Tibbitt,[†,§] April M. Kloxin,[†,‡,∥] Lisa A. Sawicki,[†,∥] and Kristi S. Anseth[†,‡,§,*]

[†]Department of Chemical and Biological Engineering, University of Colorado Boulder, Boulder, Colorado 80303, United States
[‡]Howard Hughes Medical Institute, University of Colorado Boulder, Boulder, Colorado 80303, United States
[§]BioFrontiers Institute, University of Colorado Boulder, Boulder, Colorado 80303, United States

ABSTRACT: The relationship between polymeric hydrogel microstructure and macroscopic properties is of specific interest to the materials science and polymer science communities for the rational design of materials for targeted applications. Specifically, research has focused on elucidating the role of network formation and connectivity on mechanical integrity and degradation behavior. Here, we compared the mechanical properties of chain- and step-polymerized, photodegradable hydrogels. Increased ductility, tensile toughness, and shear strain to yield were observed in step-polymerized hydrogels, as compared to the chain-polymerized gels, indicating that increased homogeneity and network cooperativity in the gel backbone improves mechanical integrity. Furthermore, the ability to degrade the hydrogels in a controlled fashion with light was exploited to explore how hydrogel microstructure influences photodegradation and erosion. Here, the decreased network connectivity at the junction points in the step-polymerized gels resulted in more rapid erosion. Finally, a relationship between the reverse gelation threshold and erosion rate was developed for the general class of photodegradable hydrogels. In all, these studies further elucidate the relationship between hydrogel formation and microarchitecture with macroscale behavior to facilitate the future design of polymer networks and degradable hydrogels, as well as photoresponsive materials such as cell culture templates, drug delivery vehicles, responsive coatings, and anisotropic materials.

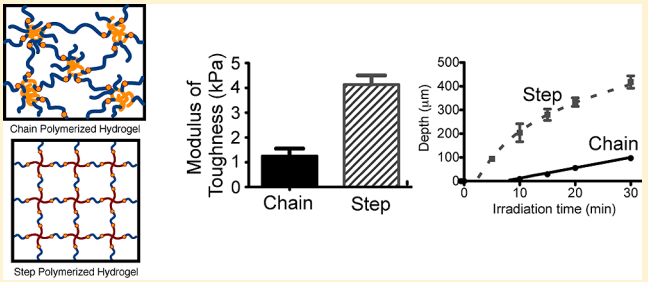

INTRODUCTION

Covalently cross-linked hydrogels are applied as cell culture templates,[1,2] absorbent materials, nonfouling coatings,[3] contact lenses,[4] and drug delivery vehicles.[5] Owing to high water content, reasonable transport of small molecules, and robust mechanical properties, covalently cross-linked hydrogels are particularly attractive materials for a broad array of biological and cellular applications. These reticulated polymer networks are formed by chemical cross-linking of hydrophilic macromolecules, such as synthetically derived poly(ethylene glycol) (PEG) or poly(vinyl alcohol) and naturally derived hyaluronic acid, gelatin, or alginate, often mildly and in the presence of cells.[6] Despite the prevalence of hydrogels in the biomedical sciences, the manner by which the cross-linking mechanism and resultant microarchitecture of the hydrogel influences the macroscopic properties (e.g., strength, toughness, and degradation) is still not fully elucidated. A better understanding of the structure–function relationship in hydrogel performance would enable improved rational design of materials for a range of targeted applications.

Cross-linked, synthetic hydrogels have been formed traditionally through a free-radical initiated chain polymerization of telechelic monomers (e.g., diacrylated PEG or 2-hydroxy ethyl methacrylate copolymerized with diethylene glycol dimethacrylate).[7] In this manner, hydrogels have been fabricated rapidly with tunable material properties[8] and have been functionalized with adhesion peptides and degradation sites.[9] However, radical initiated chain polymerizations are limited in that they are inhibited by oxygen,[10] proceed with complex kinetics,[11] can be damaging to nucleic acids and proteins,[12,13] and inherently introduce inhomogeneities into the network structure.[14,15] These inhomogeneities compromise the material properties as stress is focused on weak portions of the network, reducing the macroscopic integrity of the hydrogel.[15] Furthermore, hydrogels formed by chain polymerization degrade with heterogeneous byproducts.

Recent work has focused on the formation of cross-linked hydrogels with more ideal and homogeneous microstructures to improve network cooperativity and increase hydrogel mechanical integrity.[15−18] This has been achieved through the step polymerization of complementary, end-terminated comonomers. Originally, Hubbell and co-workers demonstrated the formation of step-polymerized hydrogels by cross-linking thiol and electron-poor, vinyl functionalized PEG-based molecules for drug delivery and cell encapsulation.[19,20] This paradigm has been extended to fabricate gels utilizing several different step

Received: December 7, 2012
Revised: March 13, 2013
Published: March 25, 2013

   dx.doi.org/10.1021/ma302522x | *Macromolecules* 2013, 46, 2785−2792

growth reactions and associated functional groups, including the copper-catalyzed, Huisgen azide−alkyne coupling of functionalized PEG-based comonomers,[16,21,22] the coupling of propylamine terminated PEG with succinimidyl glutarate terminated PEG,[15] and the photoinitiated thiol−ene coupling of norbornene functionalized PEG with dithiol peptides.[23] Uniquely, Deforest et al. demonstrated the formation of step-polymerized hydrogels through the copper-free, strain promoted azide alkyne cycloaddition (SPAAC), forming hydrogels in a bio-orthogonal and cytocompatible manner.[24] Seminal mechanical analyses of step-polymerized gels have found that these networks possess increased tensile extension[16,18] as compared to chain-polymerized analogues, while SANS data have demonstrated that these networks, although still not perfectly ideal, possess fewer heterogeneities in the network microstructure.[17] While differences between chain and step polymerization mechanisms and resultant hydrogels are clear, there is little literature on the direct comparison of mechanics and degradation between chain-polymerized and step-polymerized hydrogels. One can gain valuable insight of the structure−function relationship of hydrogels through direct comparisons between chain- and step-polymerized hydrogels with similar chemical structures but profoundly different network connectivities, which will enable the rational design and application of unique hydrogel-based materials.

Furthermore, there is a growing interest in controlling the material properties of both step- and chain-polymerized hydrogels dynamically and in a user-defined fashion using cleavable chemistries whose degradation can be triggered exogenously. Toward this end, recent work has presented a class of photodegradable hydrogels whose physical and chemical properties can be modified by light postfabrication with full spatial and temporal control.[21,25−29] Photodegradable hydrogels are appropriate for a myriad of applications in the biomedical and materials sciences. Within the tissue engineering field there is a particular interest in designing cytocompatible, photodegradable hydrogels that allow the experimenter to control the extracellular microenvironment in the presence of cells in 3D and in real time.[29−33] Meanwhile, the drug delivery community is exploiting photodegradable hydrogels to release factors at specific locations and at precise times.[34,35] For photodegradable hydrogels to be utilized most effectively in the broad range of applications, a precise and predictable understanding of how irradiation *and* network structure influence degradation-induced changes in material properties is required. In addition, photodegradation suggests unique opportunities to perform experiments that might provide a better understanding as to how network structure influences material properties during temporally regulated changes to the hydrogel structure.

This work presents the synthesis and characterization of hydrogel networks that are formed by both chain and step polymerizations of a single photodegradable PEG-based macromolecular precursor as model systems to understand differences in both mechanical properties and degradation between the resultant network structures. The formation and associated material properties of the hydrogels are investigated and compared. Furthermore, the photolabile linker in the hydrogel is employed to compare and contrast the photodegradation-induced changes in the two gels. A previously developed statistical-kinetic model of photodegradation is adapted and expanded to describe the degradation of step growth networks. This model accurately describes degradation differences between hydrogels formed by chain and step growth mechanisms, elucidating aspects of the structure−function relationship in hydrogel photodegradation. In all, the material chemistry enables a more robust understanding of how network connectivity and gel architecture influence properties and degradation, and this fundamental understanding should translate into an improved design of hydrogel cells carriers and drug delivery vehicles for biomedical applications.

■ MATERIALS AND METHODS

All reagents were purchased from Sigma-Aldrich and used as received except as otherwise noted.

Synthesis of Gel-Forming Monomers. A photolabile, acrylate functionalized monomer, poly(ethylene glycol) diphotodegradable acrylate (PEGdiPDA), was synthesized according to previous published protocols.[25,27] Briefly, an acrylated, *o*-nitrobenzyl ether was synthesized and coupled to poly(ethylene glycol) Bisamine (M_n ∼ 3400 Da; Laysan Bio Inc.) to generate a photoresponsive monomer that is capable of forming both chain- and step-polymerized networks. Four-arm poly(ethylene glycol) macromolecules (M_n ∼ 10 kDa and M_n ∼ 5 kDa; JenKem Technology USA) functionalized with thiol end groups (PEG4SH) were synthesized according to a previously published protocol.[36]

Fabrication of Chain-Polymerized Hydrogels. Chain-polymerized hydrogels were fabricated by copolymerizing PEGdiPDA with monoacrylated poly(ethylene glycol) (M_n ∼ 400 Da, PEGA; Monomer-Polymer Dajac Laboratories) via redox-initiated, free-radical chain polymerization. Stock solutions of the gel-forming precursors were prepared: 49 mM PEGdiPDA in PBS, 1 M PEGA in PBS, 2 M ammonium persulfate (APS) in PBS, and 2 M tetramethylethylenediamine (TEMED) in PBS. Three chain-polymerized hydrogels were fabricated for this work by varying the ratio of PEGdiPDA to PEGA at a constant total polymer wt % of 15 wt %. PEGdiPDA and PEGA were combined in PBS at final solution concentrations of 26.5 mM and 105 mM, respectively to form gel **a**. PEGdiPDA and PEGA were combined in PBS at final solution concentrations of 17.2 mM and 200 mM, respectively to form gel **b**. PEGdiPDA and PEGA were combined in PBS at final solution concentrations of 12.3 mM and 250 mM, respectively to form gel **c**. To initiate polymerization, APS and then TEMED were added to each solution while vortexing at final solution concentrations of 0.2 and 0.1 M, respectively. The solutions were reacted for ∼7 min to achieve complete polymerization, upon which the gels were swelled in PBS. Gels were formed *in situ* on a parallel-plate shear rheometer (50 μm thick; TA Instruments Ares 4400) or between glass slides separated by 0.5 − 1.5 mm thick silicon rubber gaskets.

Fabrication of Step-Polymerized Hydrogels. Step-polymerized hydrogels were fabricated by copolymerizing PEGdiPDA with thiol-functionalized, four-arm poly(ethylene glycol) (PEG4SH; M_n ∼ 5K or 10K) via base-catalyzed, Michael-addition. Stock solutions of the gel-forming precursors were prepared: 49 mM PEGdiPDA in PBS pH 8.0, 20 mM PEG4SH 10K in PBS pH 8.0, 40 mM PEG4SH 5K in PBS pH 8.0, and 1 M triethanolamine (TEOHA) in PBS pH 8.0. Three step-polymerized hydrogels were fabricated for this work by varying the molecular weight of the PEG4SH (5K or 10K) and altering the ratio of acrylates to thiols at a constant total polymer wt % of 10 wt %. PEGdiPDA and PEG4SH 10K were combined in PBS pH 8.0 at final solution concentrations of 11 mM and 5.5 mM (r = 1), respectively to form gel **d**. PEGdiPDA and PEG4SH 10K were combined in PBS pH 8.0 at final solution concentrations of 9.8 mM and 6.0 mM (r = 0.83), respectively to form gel **e**. PEGdiPDA and PEG4SH 5K were combined in PBS pH 8.0 at final solution concentrations of 15.2 mM and 7.6 mM (r = 1), respectively to form gel **f**. To accelerate polymerization, TEOHA was added to each solution while vortexing at a final solution concentration of 0.3 M.[20] The solution were reacted for ∼25 min to achieve complete polymerization, upon which the gels were swelled in PBS. Gels were formed *in situ* on a parallel-plate shear rheometer (50 μm thick; TA Instruments Ares 4400) or between glass slides separated by 0.5−1.5 mm thick silicon rubber gaskets.

dx.doi.org/10.1021/ma302522x | *Macromolecules* 2013, 46, 2785−2792

Modulus Measurements of Hydrogels. *In situ* polymerization was quantified with time sweep tests on gelling solutions in a parallel-plate shear rheometer (TA Instruments Ares 4400; 8.0 mm diameter and 0.05 mm height). Time sweep tests were conducted at 10 rad/s with 10% strain, which was determined to be in the linear viscoelastic regime for both chain- and step-polymerized hydrogels. Polymerization was followed until the shear storage modulus (G') reached a plateau (n = 3 for each gel type). Young's modulus was reported as three times the shear storage modulus based on the poisson ratio for PEG-based hydrogels.

Swelling Ratio Measurements of Hydrogels. For each gel type, gel samples (n = 6) were swollen and weighed in the equilibrium swollen state. The gels were subsequently lyophilized to remove the water weight from the samples and the dry weight was measured. The ratio of the equilibrium swollen weight to the dry weight was used to calculate q, the mass swelling ratio. The volumetric swelling ratio, Q, was then calculated from the mass swelling ratio.[37]

Tensile Testing of Hydrogels. Tensile testing of chain- and step-polymerized hydrogels (n = 3 for each gel type) was performed in uniaxial extension with a materials tester (MTS Synergie 100) with a 10 N load head. Swollen hydrogels were cut into ~5 mm × ~ 25 mm rectangles, and the width, length, and thickness of each sample was measured with digital calipers prior to analysis. Each sample was fixed on the materials tester by compression clamps at the top and bottom of the sample (~5 mm from each end of the gel), and the local environment was kept humidified during the analyses. The initial separation distance was measured with digital calipers, and a constant strain rate of 0.15 mm/mm/min was applied to the sample to failure. The load, stress, strain, and elongation values recorded were used to calculate the stress and strain from the measured dimensions of each sample. The percent strain at failure was calculated as the final extension divided by the initial separation distance multiplied by 100, and the toughness was calculated by numerically integrating for the area under the stress−strain curve.

Shear Testing of Hydrogels. To determine the shear strain to yield for each of the hydrogels, hydrogel samples (n = 3 for each gel type) were polymerized *in situ* on a parallel plate rheometer (TA Instruments Discovery). Once the gels reached complete polymerization, a strain sweep was performed from 1% to 1000% strain at a constant frequency of 2.5 rad/s while monitoring the storage modulus (G') and the loss modulus (G'') values. Shear strain to yield was characterized as the strain at which the value of the storage modulus fell below the value of the loss modulus.

Degradation of Hydrogels. The kinetics of the photodegradation reaction in both chain- and step-polymerized hydrogels was quantified by irradiating (λ = 365 nm; I_0 = 20 mW/cm^2) *in situ* polymerized gels on a parallel-plate shear rheometer (TA Instruments Ares 4400) and following the modulus evolution as a function of irradiation time. The normalized modulus G'/G'_0 is proportional to the normalized number density of elastically active network strands ν/ν_0, where ν is the number density of elastically active network strands, for each gel system. As irradiation cleaves bonds within the NBE moiety in the PEGdiPDA molecule, elastically active network strands are broken and based on polymer physics and photoreaction kinetics:

$$\frac{G'}{G'_0} = \frac{\nu}{\nu_0} = \exp(-kt)$$

where

$$k = \frac{\phi\varepsilon I_0}{N_A h\nu} = k_{eff} I_0$$

Here, ϕ is the quantum yield of the NBE moiety; ε is the molar absorptivity of the NBE moiety at the wavelength of irradiation (ε = 4300 L mol^{-1} cm^{-1} for λ = 365 nm); I_0 is the incident irradiation intensity (W cm^{-2}); N_A is Avogadro's number; h is the Planck constant; ν is the frequency at the wavelength of irradiation; k_{eff} is the effective rate constant by gathering all variables except for I_0. A linear fit of $\ln(G'/G'_0)$, as measured by the rheometry experiments, as a function of irradiation time was employed to calculate k and, thus, k_{eff} for both chain- and step-polymerized hydrogels. Even though these gels are optically thick (A > 0.1), similar methods to use rheometry to quantify photodegradation kinetics in other optically thick gels have been verified by NMR on optically thin samples, demonstrating that this is a viable technique for assessing degradation kinetics.[29,38]

Degradation with Collimated Light. Collimated light was delivered from an Omnicure S1000 with an internal 365 nm filter through a liquid filled light guide and collimating lens. (All irradiation equipment was purchased from EXFO.) Irradiation intensities for all degradation experiments were measured with a calibrated radiometer (Model IL1400A, International Light, Inc., Newburyport, MA), and attenuation of light by the rheometer or photomasks was accounted for by increasing the incident light intensity so that the transmitted light was at the desired intensity.

Erosion of Channels into Hydrogel Surfaces. Photopatterns (400 μm wide black lines spaced by 400 μm) were originally drawn in Adobe Illustrator and printed on Mylar (Advance Reproductions, North Andover, MA). The photopatterns were attached to glass slides with double-sided tape. Swollen chain- and step-polymerized gels (10 mm × 10 mm × 1 mm) were aligned under the channel patterns and surrounded by PBS to maintain hydration and facilitate dissolution of degraded products during patterning. The gels were then exposed to collimated 365 nm light at 10 mW/cm^2 for up to 30 min (Omnicure S1000 with 365 nm filter, liquid filled light guide, and collimating lens, EXFO). Depths of the patterned channels were verified with a profilometer (Stylus Profiler, Dektak 6M).

Model predictions. A statistical-kinetic model of photodegradation[38] in chain-polymerized networks was applied to model the erosion depth as a function of time for the chain-polymerized hydrogels in this work. This model was extended to describe photodegradation in step growth networks by altering the statistical assumptions of network connectivity to account for the differences in network structure. Furthermore, as the time scale of erosion is much faster for step-polymerized hydrogels than chain-polymerized an additional dissolution assumption was included. Briefly, this states that eroded products at the surface of the gel do not instantly diffuse out of the light path, but diffuse through the PBS solution in the light path to a solution sink at the original surface of the gel. By including this simple assumption, the statistical-kinetic model was able to describe the erosion depth as a function of irradiation time in both chain- and step-polymerized hydrogels.

Statistics. All data is reported as mean ± s.e.m.

RESULTS AND DISCUSSION

Formation of Chain- and Step-Polymerized Photodegradable Hydrogels. Photodegradable hydrogels were synthesized via chain- and step polymerization. Chain-polymerized (CP) hydrogels were formed by reacting the tetrafunctional PEGdiPDA with a difunctional comonomer, PEGA, under redox-initiated free-radical chain polymerization. Step-polymerized (SP) hydrogels were formed by reacting the difunctional PEGdiPDA with a tetrafunctional comonomer, PEG4SH, through a base-catalyzed Michael addition. In each case, the network formation occurred through the chemical bonding of the acrylate-functionalized PEGdiPDA. In the chain polymerization each acrylate is difunctional allowing the PEGdiPDA to serve as a tetrafunctional cross-linker, whereas in the step polymerization each acrylate is monofunctional extending the elastically active chains between the tetrafunctional PEG4SH cross-linkers.

Previous studies have shown that the network microstructure of PEG gels formed by chain polymerization is comprised of dense polyacrylate kinetic chains connected by PEG cross-links.[14] These heterogeneities exist on the length scale of the PEG cross-linker, while further heterogeneities form as radical initiation stochastically leads to regions of increased cross-linking density on the micrometer scale. In contrast, PEG

dx.doi.org/10.1021/ma302522x | Macromolecules 2013, 46, 2785−2792

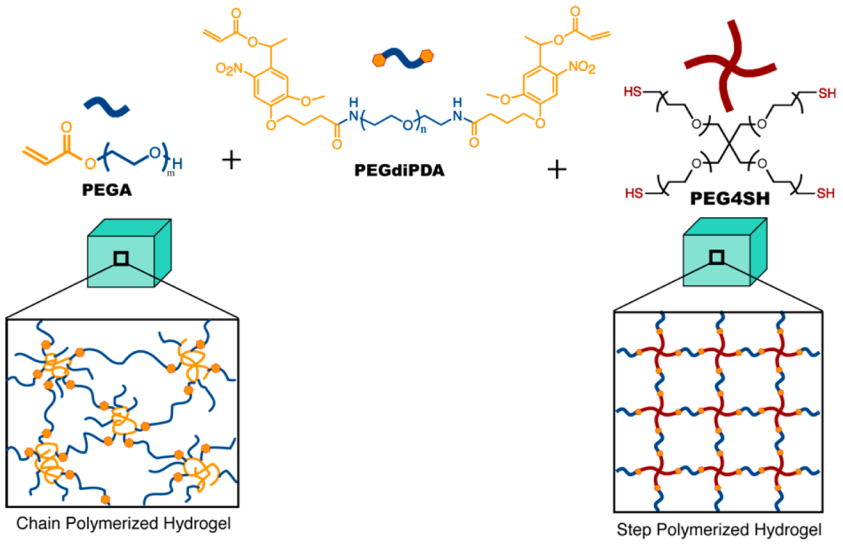

Figure 1. Fabrication of chain- and step-polymerized photodegradable hydrogels. Chain-polymerized and step-polymerized hydrogels were formed with the same photolabile monomer, PEGdiPDA. Chain-polymerized hydrogels (CP gels) were fabricated through the copolymerization of PEGdiPDA with PEGA via free-radical polymerization, resulting in a heterogeneous network structure. Step-polymerized hydrogels (SP gels) were fabricated through the copolymerization of PEGdiDPA with PEG4SH via Michael-addition polymerization.

Table 1. Physical measurements of Chain- and Step-Polymerized Hydrogels[a]

gel formulation			gel characterization					
chain	PEGdiPDA (mM)	PEGA (mM)	polymer wt %	E (kPa)	Q	tensile strain to failure (%)	tensile toughness (kPa)	shear strain to yield (%)
a	26.5	105	15	19.7 ± 1.5	11.5 ± 0.2	33 ± 4	2.2 ± 0.2	89 ± 6
b	17.2	200	15	19.5 ± 0.7	18.0 ± 1.5	33 ± 5	1.3 ± 0.3	130 ± 1
c	12.3	250	15	17.5 ± 1.8	14.1 ± 0.1	20 ± 3	0.5 ± 0.2	93 ± 4
gel formulation			gel characterization					
step	PEGdiPDA (mM)	PEG4SH (mM; Da)	polymer wt %	E (kPa)	Q	tensile strain to failure (%)	tensile toughness (kPa)	shear strain to yield (%)
d	11.0	5.5; 10K	10	14.3 ± 1.5	20.0 ± 0.8	129 ± 11	4.1 ± 0.2	420 ± 40
e	9.8	6.0; 10K	10	14.8 ± 2.8	18.1 ± 0.1	87 ± 15	6.0 ± 1.4	500 ± 70
f	15.2	7.6; 5K	10	10.1 ± 2.5	14.5 ± 0.3	112 ± 6	14.5 ± 2.0	290 ± 70

[a]The formulations for chain-polymerized (**a**–**c**) and step-polymerized (**d**–**f**) hydrogels are detailed in the Materials and Methods section. PEG4SH is presented as concentration (mM) and molecular weight (M_n in daltons).

hydrogels formed by step polymerizations have been shown to possess fewer heterogeneities on all length scales.[15] These heterogeneities are limited generally to cyclization and dangling ends. In this manner, the chain polymerization (CP) of PEGdiPDA formed a heterogeneous network structure,[14] while the step polymerization (SP) formed a more ideal network structure (Figure 1).[17]

In this study, three chain-polymerized (**a**–**c**) and three step-polymerized (**d**–**f**) hydrogels were fabricated from an array of macromolecular solutions (Table 1). It is difficult to generate chain- and step-polymerized hydrogels with directly comparable properties as the formation mechanisms lead to differences in the length of the network chains, the degree of cyclization, and swelling behavior. Therefore, a range of materials was tested to study the effect of formation mechanism (chain or step polymerization) on mechanical properties, such as tensile strain to failure, tensile toughness, and shear strain to yield.

Hydrogels were formed for each gel system *in situ* on a parallel plate rheometer to quantify the Young's modulus (E) (Table 1) and time to complete polymerization. All hydrogels formed in less than 25 min with a Young's modulus ranging from ∼10 to 20 kPa. In all cases, the total polymerization time can be tuned by altering the initial macromer concentration and the initiator concentrations (ammonium persulfate/TEMED for the chain polymerization and triethanolamine/pH for the step polymerization). (data not shown) The volumetric swelling ratio (Q) for the hydrogels ranged from ∼12 to 20.

Mechanical Analysis of Chain- and Step-Polymerized Hydrogels. It has been suggested that the increased homogeneity and network cooperativity of SP hydrogels results in an increase in mechanical integrity, specifically tensile strain to break, as compared to CP hydrogels.[16] Here, network cooperativity is used to describe the ability of multiple network chains within a gel to distribute mechanical stress cooperatively over the network chains. To compare the tensile properties of the chain- and step-polymerized PEG hydrogels studied in this work, tensile testing was conducted on all gels. The percent strains to failure for CP gels were 33 ± 4%, 33 ± 5%, and 20 ± 3% for **a**, **b**, and **c**, respectively. Whereas, the percent strains to failure for SP gels were 129 ± 11%, 87 ± 15%, and 112 ± 6% for **d**, **e**, and **f**, respectively (Table 1; Figure 2a,b). These data indicated that, in all cases, the SP gels were more ductile than the CP gels. Further analysis of the tensile testing data revealed that SP gels possessed increased tensile toughness compared to

dx.doi.org/10.1021/ma302522x | *Macromolecules* 2013, 46, 2785–2792

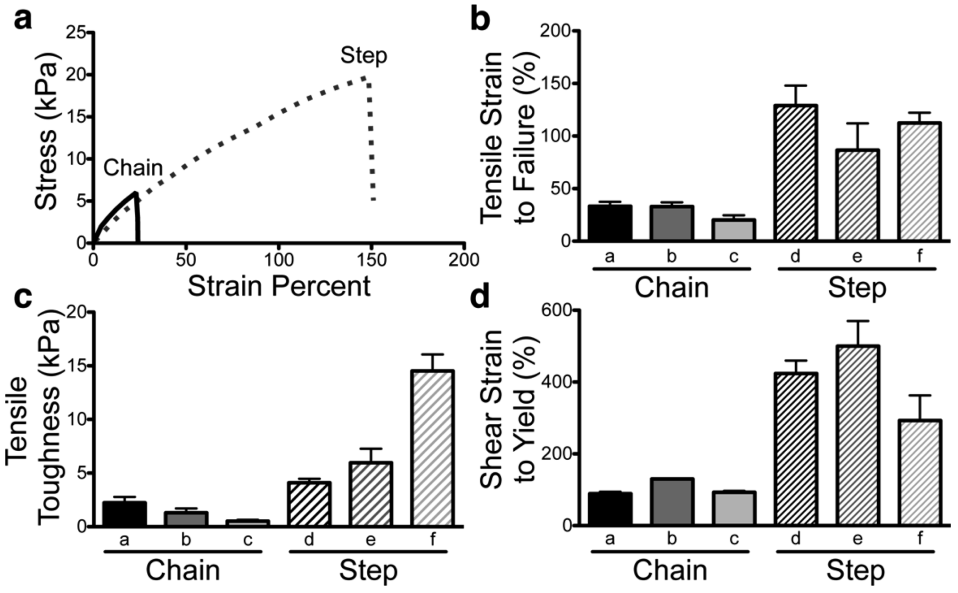

Figure 2. Mechanical analysis of chain- and step-polymerized hydrogels. (a) Uniaxial extension of CP and SP gels was conducted to measure the percent strain to failure and modulus of toughness from the stress−strain curves. Solid black line is a representative stress−strain curve for the CP gels (formulation **b**). Dotted gray line is a representative stress−strain curve for the SP gels (formulation **d**). (b) The average percent strain to failure was increased for all SP gels (dashed bars, **d**−**f**) as compared to CP gels (solid bars, **a**−**c**). (c) The SP gels (dashed bars, **d**−**f**) also possessed increased tensile toughnesses as compared to CP gels (solid bars, **a**−**c**). (d) The yield behavior of the hydrogels was analyzed on a parallel plate rheometer to determine the shear strain to yield for each sample. As with the tensile analyses, the SP gels (dashed bars, **d**−**f**) demonstrated increased shear strains to yield as compared to CP gels (solid bars, **a**−**c**) across all samples.

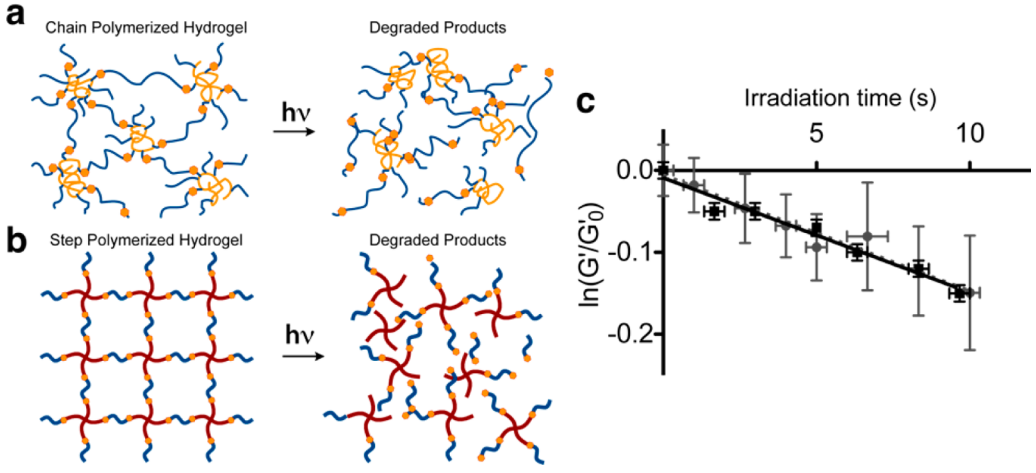

Figure 3. Photodegradation of chain- and step-polymerized hydrogels. (a and b) The *o*-nitrobenzyl ether moieties (orange ring structures) in PEGdiPDA undergo an irreversible cleavage in response to irradiation (one-photon, $\lambda \sim 320-436$ nm; two-photon, $\lambda \sim 740$ nm), breaking elastically active network strands in the hydrogel backbone. In this manner, light can be employed to degrade and, ultimately, erode the CP and SP hydrogels. (c) Owing to the inclusion of the same photolabile monomer into the network backbone, the initial effective cleavage kinetic constant, defined as the negative slope of $\ln(G/G_0)$ as a function of irradiation time divided by the incident irradiation intensity, was similar for the CP (black, formulation **b**) and SP (gray, formulation **d**) gels.

CP gels (Table 1; Figure 2a,c). Specifically, the tensile toughness of the SP gels were 4.1 ± 0.2, 6.0 ± 1.4, and 14.5 ± 2.0 kPa for **d**, **e**, and **f**, respectively, while the tensile toughness for the CP gels were 2.2 ± 0.2, 1.3 ± 0.3, and 0.5 ± 0.2 kPa for **a**, **b**, and **c**, respectively. In addition to the tensile testing, strain sweeps on *in situ* polymerized hydrogels were conducted to investigate the shear strain to yield for each of the samples. The SP gels exhibited increased shear strain to yield in all cases as compared to the CP gels (Table 1; Figure 2d), 420 ± 40, 500 ± 70, and 290 ± 70% for SP gels **d**, **e**, and **f**, respectively, and 89 ± 6, 130 ± 1, and 93 ± 4% for CP gels, **a**, **b**, and **c**, respectively.

In both the tensile and shear analyses, it was observed that mechanical integrity was improved for hydrogels formed by step polymerization as compared to chain polymerization. These differences in material properties were conferred by the network structure, specifically the increased network cooperativity and decreased heterogeneity in the SP hydrogel, and suggest that applications that require more ductile or tough materials should employ SP hydrogels. In addition to mechanical integrity, network connectivity directly relates to the diffusion of macromolecules through the hydrogel network and ideal gels should facilitate more uniform diffusion as compared to heterogeneous gels. Finally, these data suggest

dx.doi.org/10.1021/ma302522x | *Macromolecules* 2013, 46, 2785−2792

that mechanical stresses were translated anisotropically in heterogeneous, CP gels, which may be important for mechanical stimulation or differentiation of mammalian cells.

Photodegradation of Chain- and Step-Polymerized Hydrogels. The CP and SP gels were formed from the same photolabile monomer, PEGdiPDA, rendering them photodegradable. The degradation is facilitated by the *o*-nitrobenzyl ether (NBE) moieties that reside within the PEGdiPDA monomer (Figure 1) and undergo an irreversible cleavage in the presence of light (one-photon, λ = 320−436 nm; two-photon, λ = 740 nm).[27] On account of this property, light was able to cleave bonds within the materials, resulting in the breakage of elastically active network strands and, ultimately, erosion of the gel with light exposure (Figure 3a,b). For the analysis of photodegradation in chain- and step-polymerized hydrogels, a representative CP gel (formulation **b**) and a representative SP gel (formulation **d**) were analyzed and compared. Prior to erosion, photodegradation led to an exponential decrease in the shear storage modulus (Figure 3c), which was governed by the inherent rate of photocleavage of the NBE moiety, k_{eff}. As both of the gels contained the same NBE moiety in the network backbone, it was predicted that the initial cleavage rate of elastically active strands, measured as a decrease in shear storage modulus, would be the same for both the CP and SP gels. The cleavage rate, k_{eff}, for the CP gel was 0.0140 ± 0.0012 s^{-1} and the cleavage rate for the SP gel was 0.0142 ± 0.0012 s^{-1}. These effective cleavage rates were not statistically different and were in agreement with previously reported cleavage rates for similar NBE moieties.[25,29,32,38,39]

To investigate how network structure influences mass loss and erosion rates of the CP and SP gels, physical channels were eroded into the surfaces of both gels. While rheometry results indicated that the inherent rate of photodegradation is independent of network structure, the erosion rates for the representative CP and SP gels diverged even at short time scales (Figure 4a). Statistical-kinetic models of photodegradation and erosion in chain-polymerized[38] and step-polymerized hydrogels were applied to describe the depth of channel formation as a function of time to elucidate how network connectivity leads to dramatic differences in pattern formation rate. In both cases, the simple statistical-kinetic model captured the observed erosion behavior (Figure 4a), which indicates that the statistical-kinetic model includes the relevant physics of erosion in CP and SP photodegradable gels. These results demonstrate that the lower network connectivity observed in SP gels leads to an increased rate of erosion. For these experiments, the assumption of dissolution of erosion by-products was accounted for in the rapidly degrading step-polymerized gels (see Materials and Methods).

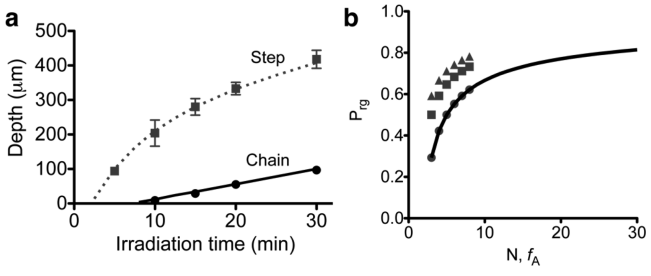

Figure 4. Modeling erosion in chain- and step-polymerized hydrogels. (a) The erosion depth of photopatterned channels as a function of irradiation time was plotted for the CP (black, formulation **b**) and SP (gray, formulation **d**) photodegradable hydrogels. A statistical-kinetic photodegradation model (solid and dashed lines for CP and SP, respectively) based on the photocleavage reaction and network connectivity agreed well with experimental data over the 30 min exposure time. (b) Critical extent of NBE moieties that need to be cleaved to reach reverse gelation governs the rate at which features can be patterned into photodegradable gels. P_{rg} is a function of network connectivity in both CP and SP gels. Here, $P_{rg}(N)$ is plotted for CP gels (solid black line) and $P_{rg}(f_A)$ is plotted for SP gels with f_B = 2 (gray circles), f_B = 3 (gray squares), and f_B = 4 (gray triangles).

In both of these models, the critical parameter that dictates the erosion rate is the critical fraction of cleaved NBE species, P_{rg}, which governs reverse gelation. Here, reverse gelation refers to the critical extent of bonds cleaved that causes the insoluble gel to erode completely into soluble polymer chains (Figure 3a,b). The network structure of the representative SP gel (formulation **b**) resulted in a P_{rg} = 0.42 while the representative CP gel (formulation **d**) resulted in a P_{rg} = 0.77. A critical time scale, t_c, was defined as the time to reach reverse gelation at the surface of a photodegradable hydrogel and is a function of P_{rg}:

$$t_c = \frac{-\ln(1 - P_{rg})}{k_{eff} I_0} \quad (1)$$

where, k_{eff} is the effective kinetic constant of cleavage of the NBE moiety; I_0 is the intensity of the incident irradiation. Since the cleavage reaction followed first-order kinetics with the same effective kinetic constant in both gels and each was exposed to the same incident irradiation, the difference in P_{rg} alone determined the difference in erosion time constants, t_c = 490 s for the CP gel and t_c = 180 s for SP gel.

The critical erosion time scale, t_c, governed not only the time to erode the surface of the gel, but also the rate at which erosion progresses through the depth of the gel. A critical length scale, z_c, was defined from the Beer-Lamber Law:

$$z_c = \frac{1}{2.3\varepsilon_i C_i} \quad (2)$$

Here ε_i is the molar absorptivity of the NBE moiety; C_i is the concentration of the NBE moiety. A rate for which the erosion progressed through the gel was calculated as the critical length scale of photodegradation divided by the critical time scale of photodegradation:

$$\frac{z_c}{t_c} = \frac{-k_{eff} I_0}{2.3\varepsilon_i C_i \ln(1 - P_{rg})} \quad (3)$$

Owing to the differences in the P_{rg} and the concentration of NBE moieties in the CP and SP gels, the rate of erosion was significantly faster for the SP gel as compared to the CP gel. The simple scaling analysis predicted an erosion rate of 3.6 and 18.4 μm/min compared to experimental values of 4.4 ± 0.1 and 18.6 ± 2.0 μm/min for the CP and SP gels, respectively.

The above analysis of the relationship between erosion rate and P_{rg} holds for the specific chain-polymerized and step-polymerized hydrogels in this manuscript as well as for gels formed with the same network connectivity, i.e., the same P_{rg}. However, more broadly, the equations hold for the general class of *photodegradable* hydrogels for which the network structure and physical parameters are known. Specifically, step-polymerized gels have been formed from PEG monomers with varying functionality leading to different network connectivity.[18,40] For instance, the cross-linking of an octafunc-

dx.doi.org/10.1021/ma302522x | *Macromolecules* 2013, 46, 2785−2792

tional, thiol-terminated PEG with a tetrafunctional, vinyl−sulfone-terminated PEG would form a network with different connectivity than a tetrafunctional, thiol-terminated PEG and a trifunctional, vinyl−sulfone terminated PEG. Differences in network connectivity are directly related to P_{rg} and, ultimately, the rate of erosion. The reverse gelation point for step-polymerized hydrogels, formed from two complementary monomers, has been adapted from classical derivations by Flory and Rehner that describe network formation in step growth polymerizations:[23,41,42]

$$P_{rg}^{step} = 1 - \frac{1}{\sqrt{r(f_A - 1)(f_B - 1)}} \quad (4)$$

where, f_A is the functionality of the A-terminated monomer; f_B is the functionality of the B-terminated monomer; and r is the stoichiometric ratio of A to B. This derivation based on the Flory−Rehner theory assumes complete reaction of all functional end groups in the polymer network without loops, dangling ends, or entanglements. Therefore, real systems, such as the SP gels in this work, will have an effective P_{rg} lower than the ideal calculation as loops, dangling ends, and entanglements form during polymerization. The reverse gelation point for chain-polymerized hydrogels has been adapted from classical derivations of Macosko and Miller:[43−45]

$$P_{rg}^{chain} = 1 - \frac{1}{\sqrt{N - 1}} \quad (5)$$

where, N is the number of cross-linking molecules per polyacrylate kinetic chain, which is determined by the polymerization conditions and monomer formulation. Equations 4 and 5 indicate how network connectivity relates to P_{rg}, which can be related to the rate of erosion in photodegradable hydrogels (eq 3).

Figure 4b illustrates how P_{rg} is related to the monomers or polymerization conditions for both chain- and step-polymerized hydrogels (r was assumed to be unity for all step polymerization conditions; Figure 4b). For a multifunctional monomer reacting with a difunctional monomer through step polymerization (Figure 4b, gray circles), P_{rg} collapses onto the curve for the chain polymerization. However, chain polymerizations typically result in an N of 10−100, while it is difficult to synthesize multifunctional monomers beyond a functionality of 8 for step polymerizations ($f_A \leq 8$). Therefore, to achieve reverse gelation points that are similar to common chain-polymerized formulations, one can copolymerize multifunctional monomers (f_A = 3−8) with trifunctional or tetrafunctional complementary monomers (Figure 4b; gray squares and triangles, respectively).

This analysis demonstrates how network structure relates to the rates of erosion or feature generation in photodegradable hydrogels. By exploiting the rapid erosion of step-polymerized hydrogels formed by the copolymerization of complementary tetrafunctional and difunctional monomers, photodegrading hydrogels were designed for the controlled release entrapped factors[35] and cells,[29] as well as geometric patterning of cell culture microwells.[46] Further, the increased P_{rg} for CP gels is advantageous to generate materials with broad anisotropic elasticities in the x−y[30] or z-dimensions[31] as the gel remains intact at a lower cross-linking density than the SP gels.

CONCLUSION

Photodegradable hydrogels were fabricated by both chain and step polymerization from the same photolabile monomer, PEGdiPDA. Compared to chain-polymerized gels, step-polymerized hydrogels possessed increased mechanical integrity, as quantified by ductility, tensile toughness, and shear strain to yield. Increases in mechanical integrity were attributed to increased homogeneity and network cooperativity possessed in step-polymerized hydrogels as compared to the relatively heterogeneous chain-polymerized gels. Light-induced degradation and erosion was demonstrated in both the chain-polymerized and step-polymerized gels. The inherent kinetic constant of photodegradation was the same in the two systems as both gels possess the same *o*-nitrobenzyl ether moiety in their backbones, while the rate of erosion was much faster in step-polymerized hydrogels on account of the relatively lower network connectivity. Taken together, these studies illustrate the utility of photodegradable hydrogels polymerized by either chain or step growth polymerization and provide quantitative tools for designing unique photodegradable gels and predicting their degradation and erosion, critical parameters for regulating cell fate,[47] tissue regeneration,[48] and drug release[5] among many other biomedical applications.

AUTHOR INFORMATION

Corresponding Author

*E-mail: (K.S.A.) kristi.anseth@colorado.edu..

Present Address

∥(A.M.K.) Departments of Chemical and Biomolecular Engineering and Materials Science and Engineering, University of Delaware, Newark, Delaware 19716, United States

Notes

The authors declare no competing financial interest.

ACKNOWLEDGMENTS

The authors thank Prof. Christopher N. Bowman for generous use of the DekTak Profilometer and Dr. Kelly M. Schultz for assistance with the shear strain to yield measurements. Fellowship assistance to M.W.T. was awarded by the US Department of Education's Graduate Assistantships in Areas of National Need, an NIH Molecular Biophysics Training Grant (T32 GM-065103), and the Teets Family Endowed Doctoral Fellowship. This work was made possible by financial support from the National Science Foundation (DMR 1006711) and the Howard Hughes Medical Institute.

REFERENCES

(1) Lutolf, M. P.; Hubbell, J. A. *Nat. Biotechnol.* **2005**, *23*, 47−55.
(2) Tibbitt, M. W.; Anseth, K. S. *Biotechnol. Bioeng.* **2009**, *103*, 655−663.
(3) Magin, C. M.; Finlay, J. A.; Clay, G.; Callow, M. E.; Callow, J. A.; Brennan, A. B. *Biomacromolecules* **2011**, *12*, 915−922.
(4) Kidane, A.; Szabocsik, J. M.; Park, K. *Biomaterials* **1998**, *19*, 2051−2055.
(5) Liechty, W. B.; Kryscio, D. R.; Slaughter, B. V.; Peppas, N. A. *Annu. Rev. Chem. Biomol. Eng.* **2010**, *1*, 149−173.
(6) Peppas, N. A.; Hilt, J. Z.; Khademhosseini, A.; Langer, R. *Adv. Mater.* **2006**, *18*, 1345−1360.
(7) Sawhney, A. S.; Pathak, C. P.; Hubbell, J. A. *Macromolecules* **1993**, *26*, 581−587.
(8) Anseth, K. S.; Bowman, C. N.; BrannonPeppas, L. *Biomaterials* **1996**, *17*, 1647−1657.
(9) West, J. L.; Hubbell, J. A. *Macromolecules* **1999**, *32*, 241−244.

(10) Hoyle, C. E.; Bowman, C. N. *Angew. Chem., Int. Ed.* **2010**, *49*, 1540−1573.
(11) Anseth, K. S.; Wang, C. M.; Bowman, C. N. *Polymer* **1994**, *35*, 3243−3250.
(12) Quick, D. J.; Anseth, K. S. *J. Controlled Release* **2004**, *96*, 341−351.
(13) McCall, J. D.; Lin, C. C.; Anseth, K. S. *Biomacromolecules* **2011**, *12*, 1051−1057.
(14) Lin-Gibson, S.; Jones, R. L.; Washburn, N. R.; Horkay, F. *Macromolecules* **2005**, *38*, 2897−2902.
(15) Sakai, T.; Matsunaga, T.; Yamamoto, Y.; Ito, C.; Yoshida, R.; Suzuki, S.; Sasaki, N.; Shibayama, M.; Chung, U. I. *Macromolecules* **2008**, *41*, 5379−5384.
(16) Malkoch, M.; Vestberg, R.; Gupta, N.; Mespouille, L.; Dubois, P.; Mason, A. F.; Hedrick, J. L.; Liao, Q.; Frank, C. W.; Kingsbury, K.; Hawker, C. J. *Chem. Commun.* **2006**, 2774−2776.
(17) Matsunaga, T.; Sakai, T.; Akagi, Y.; Chung, U.; Shibayama, M. *Macromolecules* **2009**, *42*, 1344−1351.
(18) Yang, T.; Long, H.; Malkoch, M.; Gamstedt, E. K.; Berglund, L.; Hult, A. *J. Polym. Sci., Polym. Chem.* **2011**, *49*, 4044−4054.
(19) Elbert, D. L.; Pratt, A. B.; Lutolf, M. P.; Halstenberg, S.; Hubbell, J. A. *J. Controlled Release* **2001**, *76*, 11−25.
(20) Lutolf, M. P.; Raeber, G. P.; Zisch, A. H.; Tirelli, N.; Hubbell, J. A. *Adv. Mater.* **2003**, *15*, 888−892.
(21) Johnson, J. A.; Baskin, J. M.; Bertozzi, C. R.; Koberstein, J. T.; Turro, N. J. *Chem. Commun.* **2008**, 3064−3066.
(22) Johnson, J. A.; Finn, M. G.; Koberstein, J. T.; Turro, N. J. *Macromolecules* **2007**, *40*, 3589−3598.
(23) Fairbanks, B. D.; Schwartz, M. P.; Halevi, A. E.; Nuttelman, C. R.; Bowman, C. N.; Anseth, K. S. *Adv. Mater.* **2009**, *21*, 5005−5010.
(24) DeForest, C. A.; Polizzotti, B. D.; Anseth, K. S. *Nat. Mater.* **2009**, *8*, 659−664.
(25) Kloxin, A. M.; Kasko, A. M.; Salinas, C. N.; Anseth, K. S. *Science* **2009**, *324*, 59−63.
(26) Frey, M. T.; Wang, Y. L. *Soft Matter* **2009**, *5*, 1918−1924.
(27) Kloxin, A. M.; Tibbitt, M. W.; Anseth, K. S. *Nature Protocols* **2010**, *5*, 1867−1887.
(28) Wong, D. Y.; Griffin, D. R.; Reed, J.; Kasko, A. M. *Macromolecules* **2010**, *43*, 2824−2831.
(29) DeForest, C. A.; Anseth, K. S. *Nature Chem.* **2011**, *3*, 925−931.
(30) Kloxin, A. M.; Benton, J. A.; Anseth, K. S. *Biomaterials* **2010**, *31*, 1−8.
(31) Kloxin, A. M.; Tibbitt, M. W.; Kasko, A. M.; Fairbairn, J. F.; Anseth, K. S. *Adv. Mater.* **2010**, *22*, 61−66.
(32) Tibbitt, M. W.; Kloxin, A. M.; Dyamenahalli, K. U.; Anseth, K. S. *Soft Matter* **2010**, *6*, 5100−5108.
(33) DeForest, C. A.; Anseth, K. S. *Angew. Chem., Int. Edit.* **2012**, *51*, 1816−1819.
(34) Peng, K.; Tomatsu, I.; van den Broek, B.; Cui, C.; Korobko, A. V.; van Noort, J.; Meijer, A. H.; Spaink, H. P.; Kros, A. *Soft Matter* **2011**, *7*, 4881−4887.
(35) Tibbitt, M. W.; Han, B. W.; Kloxin, A. M.; Anseth, K. S. *J. Biomed. Mater. Res. Part A* **2012**, *100A*, 1647−1654.
(36) Fairbanks, B. D.; Singh, S. P.; Bowman, C. N.; Anseth, K. S. *Macromolecules* **2011**, *44*, 2444−2450.
(37) Bryant, S. J.; Anseth, K. S. In *Scaffolding in Tissue Engineering*; Ma, P. X., Elisseeff, J., Eds.; Marcel Dekker, Inc.: New York, 2005; pp 69−88.
(38) Tibbitt, M. W.; Kloxin, A. M.; Anseth, K. S. *J. Polym. Sci., Polym. Chem.* **2013**, in press.
(39) Griffin, D. R.; Patterson, J. T.; Kasko, A. M. *Biotechnol. Bioeng.* **2010**, *107*, 1012−1019.
(40) Gould, S. T.; Darling, N. J.; Anseth, K. S. *Acta Biomater.* **2012**, *8*, 3201−3209.
(41) Flory, P. J. *Principles of Polymer Chemistry*; Cornell University Press: Ithaca, NY, 1953.
(42) Flory, P. J.; Rehner, J. *J. Chem. Phys.* **1943**, *11*, 512−520.
(43) Macosko, C. W.; Miller, D. R. *Macromolecules* **1976**, *9*, 199−206.
(44) Miller, D. R.; Macosko, C. W. *Macromolecules* **1976**, *9*, 206−211.
(45) Reddy, S. K.; Anseth, K. S.; Bowman, C. N. *Polymer* **2005**, *46*, 4212−4222.
(46) Kloxin, A. M.; Lewis, K. J. R.; DeForest, C. A.; Seedorf, G.; Tibbitt, M. W.; Balasubramaniam, V.; Anseth, K. S. *Integr. Biol.* **2012**, *4*, 1540−1549.
(47) Anderson, S. B.; Lin, C. C.; Kuntzler, D. V.; Anseth, K. S. *Biomaterials* **2011**, *32*, 3564−3574.
(48) Bryant, S. J.; Anseth, K. S. *J. Biomed. Mater. Res. Part A* **2003**, *64A*, 70−79.